Chemistry Letters Vol.47, No.11 (2018)

Superior Electrochemical Performance of a Ni–P/Si Negative Electrode for Li-ion Batteries in an Ionic Liquid Electrolyte

Kazuki Yamaguchi, Yasuhiro Domi, Hiroyuki Usui, Ayumu Ueno, Takuro Komura, Toshiki Nokami, Toshiyuki Itoh, and Hiroki Sakaguchi*

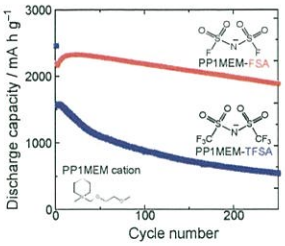

An annealed Ni–P/(etched Si) negative electrode for Li-ion batteries exhibited a higher initial discharge capacity in bis(fluorosulfonyl)amide (FSA)-based ionic liquid electrolyte, which is superior to the initial capacity in bis(trifluoromethanesulfonyl)amide (TFSA)-based electrolyte. In addition, an excellent cycle stability was also achieved. Therefore, FSA-based electrolyte can enhance the electrochemical performance of the annealed Ni–P/(etched Si) negative electrode.

Chem. Lett. **2018**, 47 doi:10.1246/cl.180649

Received: July 25, 2018 | Accepted: September 4, 2018 | Web Released: September 15, 2018 CL-180649

Superior Electrochemical Performance of a Ni–P/Si Negative Electrode for Li-ion Batteries in an Ionic Liquid Electrolyte

Kazuki Yamaguchi,[1,2] Yasuhiro Domi,[1,2] Hiroyuki Usui,[1,2] Ayumu Ueno,[1,2] Takuro Komura,[1,2] Toshiki Nokami,[1,2] Toshiyuki Itoh,[1,2] and Hiroki Sakaguchi*[1,2]

[1]*Department of Chemistry and Biotechnology, Graduate School of Engineering, Tottori University, 4-101 Minami, Koyama-cho, Tottori 680-8552, Japan*

[2]*Center for Research on Green Sustainable Chemistry, Tottori University, 4-101 Minami, Koyama-cho, Tottori 680-8552, Japan*

E-mail: sakaguch@tottori-u.ac.jp

To achieve electrode performance with both high capacity and long cycle life, we investigated the effect of the anion structure in an ionic liquid electrolyte on the electrochemical performance of an annealed Ni–P/(etched Si) negative electrode for Li-ion batteries. The electrode maintained a discharge capacity of 1890 mA h g^{-1} after 250 cycles in bis(fluorosulfonyl)amide-based ionic liquid electrolyte, which was approximately three times higher than that in bis(trifluoromethanesulfonyl)amide-based electrolyte.

Keywords: Ni–P-coated silicon | Ionic liquid | Li-ion batteries

To popularize electric vehicles (EVs), lithium-ion batteries (LIBs) with higher energy density have been desired. Graphite negative electrodes, which are currently used in commercial LIBs, have an insufficient capacity (372 mA h g^{-1}) for EVs application. On the other hand, silicon (Si) is a promising active material as a negative electrode material due to its remarkably high theoretical capacity of 3580 mA h g^{-1} ($Li_{15}Si_4$).[1,2] However, Si shows poor cycle stability because it goes through huge volumetric changes during lithiation/delithiation reactions,[3,4] which generates high stresses and large strains in the active material. The accumulation of strains during repeated charge-discharge cycling results in disintegration of the active material layer. To address this issue, we have developed composite electrodes such as $LaSi_2$/Si,[5] Ni–P/Si,[6,7] and TiO_2/Si,[8] which have both good cycle stability and high capacity. Among them, an electrode consisting of annealed Ni–P/(etched Si) particles exhibited an excellent cycle performance with a reversible capacity of 2000 mA h g^{-1} after 100 cycles in a conventional organic electrolyte.[7] The annealed Ni–P/(etched Si) powder is prepared by the following processes; (1) etching Si with hydrofluoric acid to remove its surface oxide, (2) coating etched Si with Ni–P consisting of Ni and Ni_3P by an electroless deposition (ELD) method, and (3) annealing Ni–P/(etched Si) at 800 °C. A Ni–P coating layer acts as a Li diffusion pathway in the active material layer, and releases the stresses. In addition, etching and annealing can enhance the adhesion between Si surface and Ni–P layer, which results in improved performance compared to an untreated Ni–P/Si electrode.

The electrolyte is one of the key components determining lifetime and safety of batteries. Ionic liquids have received much attention as an electrolyte solvent because of its excellent physicochemical properties, e.g. negligible vapor pressure, non-flammability, and a wide electrochemical window.[9–11] Since next-generation LIBs with a higher energy density need to display reduced risk of ignition or explosion, ionic liquid is promising to enhance safety.[12] We have reported that the cycle stability of a Si-alone electrode in some ionic liquid electrolytes is superior to that in a conventional organic electrolyte.[13,14]

While it was reported by some researchers that ionic liquid electrolytes can enhance the cycle performance of Si-based electrodes,[15–18] the optimization of anion structure in an ionic liquid electrolyte has not been sufficiently studied yet. We have investigated the effect of anion structure in an ionic liquid electrolyte to improve the electrochemical performance of the Si-alone negative electrode.[19] We have also found that an annealed Ni–P/(etched Si) electrode exhibits better cycle stability in an ionic liquid electrolyte of lithium bis(trifluoromethanesulfonyl)-amide/*N*-methyl-*N*-propylpyrrolidinium bis(fluorosulfonyl)-amide (LiTFSA/Py13-FSA) under a charge capacity limit.[7] However, the ionic liquid electrolyte is not necessarily the best for the electrode. In this study, to improve the electrochemical performance of annealed Ni–P/(etched Si) negative electrode for LIBs, we determined the effect of anion structure in an ionic liquid electrolyte on its performance. We adopted ionic liquid electrolytes consisting of piperidinium-based cation and amide-based anion, where the anion of the Li salt was the same as that of the ionic liquid unless otherwise stated.

We designed annealed Ni–P/(etched Si) powder, and commissioned Hitachi Metals Neomaterial, Ltd. to prepare it. Chemical etching with hydrofluoric acid was performed to remove the natural dioxide film on the Si surface accompanied by roughening of the surface. Etched Si was coated with Ni–P particles by ELD,[6] and the powders were subsequently annealed at 800 °C in an inert gas atmosphere. An annealed Ni–P/(etched Si) electrode was prepared by gas–deposition (GD) which requires no binders or conductive additives. The detailed conditions of GD have been reported previously.[13] We fabricated 2032-type coin cells consisting of annealed Ni–P/(etched Si) electrode as working electrode, Li foil (Rare Metallic, 99.90%, thickness: 1.0 mm) as counter electrode, ionic liquid electrolyte, and a glass fiber filter as separator. The areas of the active material layer and Li foil in the cell are 0.5 cm^2 and 2.0 cm^2, respectively. The electrolyte solution used in this study was 1 mol dm^{-3} (M) lithium bis(fluorosulfonyl)amide (LiFSA) dissolved in 1-((2-methoxyethoxy)methyl)-1-methylpiperidinium bis(fluorosulfonyl)amide (PP1MEM-FSA). In addition, 1 M LiTFSA dissolved in 1-((2-methoxyethoxy)methyl)-1-methylpiperidinium bis(trifluoromethanesulfonyl)amide (PP1MEM-TFSA) was adopted. The electrolyte preparation and cell assembly were conducted in an Ar–filled glove box (Miwa MFG, DBO–2.5LNKP–TS) with an oxygen concentration below 1 ppm and a dew point below −100 °C. A galvanostatic charge–

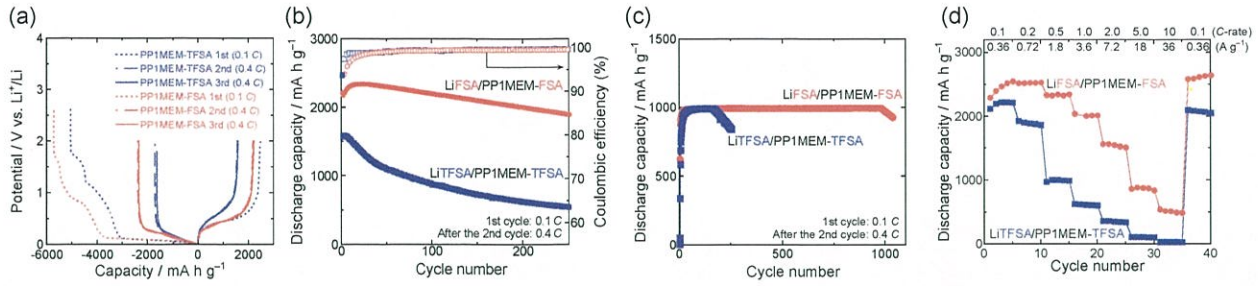

Figure 1. (a) The initial charge-discharge curves, cycling performance (b) without and (c) with charge (lithiation) capacity limit at 1000 mA h g^{-1}, and (d) rate capability of annealed Ni–P/(etched Si) electrodes in 1 M LiFSA/PP1MEM-FSA or LiTFSA/PP1MEM-TFSA.

discharge test was carried out using an electrochemical measurement system (HJ1001SM8, Hokuto Denko Co., Ltd.) in a potential range between 0.005 and 2.000 V vs. Li^+/Li at 303 K. The current density was set at 0.36 A g^{-1} (0.1 *C*) in the 1st cycle and 1.44 A g^{-1} (0.4 *C*) after the 2nd cycle. Electrochemical impedance spectroscopic (EIS) analysis was performed at 0.005 V vs. Li^+/Li in the frequency range from 100 kHz to 10 mHz with amplitude of 5 mV. We used a three-electrode cell for EIS measurement to reduce effects from the counter electrode. The surface morphologies of the annealed Ni–P/(etched Si) electrodes after charge–discharge cycle were observed with a field-emission scanning electron microscope (FE-SEM: JSM-6701F, JEOL Co., Ltd.).

Figure 1a shows the initial three charge-discharge curves of annealed Ni–P/(etched Si) electrodes in 1 M LiFSA/PP1MEM-FSA. In addition, the results in 1 M LiTFSA/PP1MEM-TFSA were also plotted. The electrode exhibited a discharge capacity of 2200 and 2400 mA h g^{-1} at the first cycle in the FSA- and TFSA-based electrolytes, respectively. In addition, a potential gradient between 0.8 and 2.0 V vs. Li^+/Li appeared on charge curves in each electrolyte, which results in a formation of surface film through reductive decomposition of the electrolyte.[19–22] Since the surface film has an insulation property and Li^+ conductivity, it can prevent the electrolyte from continuing to be reductively decomposed. Therefore, the potential gradient disappeared after the second cycle. Although the electrode showed a relatively low discharge capacity of 1560 mA h g^{-1} in the second cycle in the TFSA-based electrolyte, a discharge capacity of 2170 mA h g^{-1} was maintained in the FSA-based electrolyte. In the third cycle, discharge capacities were almost the same as those in the second cycle regardless of the electrolyte. Thus, we concluded that serious degradation of the electrode did not occur in the initial cycles.

In Figure 1b, the annealed Ni–P/(etched Si) electrode exhibited an excellent cycle stability with a discharge capacity of 1890 mA h g^{-1} in the FSA-based electrolyte even after 250 cycles. In addition, the capacity decay hardly occurred in the electrolyte. In contrast, the electrode exhibited only 540 mA h g^{-1} in the TFSA-based electrolyte after 250 cycles, which suggests that the electrode disintegrated. We proposed that the cycle stability is related to the structural stability of a surface film on the electrode. The FSA-derived film is mainly comprised of LiF which enhances structural stability of the film,[17] whereas LiF content in the TFSA-derived film is relatively low. Therefore, it is considered that the cycle stability of the electrode in the FSA-based electrolyte was superior to that in the TFSA-based electrolyte. In addition, the cycle stability of the annealed Ni–P/(etched Si) electrode was higher than that of a Si-alone electrode.[23] This is because a Ni–P coating layer accommodated stresses caused by a huge volumetric change of Si active material during charge-discharge cycle and suppressed a degradation of the active material layer. Furthermore, the cycle performance of the annealed Ni–P/(etched Si) electrode in the FSA-based electrolyte was higher than the performance of cyclized-polyacrylonitrile-based Si nanocomposite architecture (nSi-cPAN).[17] The nSi-cPAN exhibited good performance with 1400 mA h g^{-1} over 200 cycles, which is the best Si-based electrode as far as we know. Therefore, we consider that the combination of the FSA-based electrolyte with the annealed Ni–P/(etched Si) electrode can be one of the best candidates to realize next-generation LIB with a Si-based negative electrode. No drop of the Coulombic efficiency was observed regardless of the kind of electrolyte. This result indicates that drastic electrode disintegration did not occur.

We have demonstrated that yjr cycle life of a Si-alone electrode can be prolonged by controlling the amount of Li insertion–extraction.[14] Thus, we expected the cycle stability of the Ni–P/Si electrode is also improved by a charge (Li-insertion) capacity limit. Figure 1c shows the long cycle performance of the annealed Ni–P/(etched Si) electrode in ionic liquid electrolytes with a charge capacity limit of 1000 mA h g^{-1}. In the TFSA-based electrolyte, discharge capacity decayed at about 160 cycles. On the other hand, in the FSA-based electrolyte, the electrode exhibited an excellent cycle life with a reversible capacity of 1000 mA h g^{-1} over ca. 1000 cycles. Consequently, it is obvious that the anion of an ionic liquid is very important to enhance cycle stability of Si-based electrodes.

As both energy and power densities are critical factors in LIBs, we measured the rate capability of the annealed Ni–P/(etched Si) electrode, as shown in Figure 1d. In the TFSA-based electrolyte, the electrode only retained 50% of the first discharge capacity at 0.5 *C* and exhibited almost no capacity at 5.0 and 10 *C*. Potential plateaus were hardly observed in charge-discharge curves as shown in Figure S1a. In contrast, in the FSA-based electrolyte, the electrode maintained 60% of the initial capacity at 2.0 *C*, and showed a discharge capacity of 500 mA h g^{-1} even at 10 *C*, which is higher than the theoretical capacity of graphite (372 mA h g^{-1}). The plateaus also appeared in the FSA-based electrolyte, as shown in Figure S1b. When the current rate was back to 0.1 *C* at the 36th cycle, the capacities

were almost the same as the first capacity in each electrolyte. Thus, the capacity fading at the high current rate would not be attributed to the electrode deterioration. The capacity gradually decreased in the TFSA-based electrolyte in subsequent charge-discharge test at 0.1 *C*, whereas that hardly decreased in the FSA-based electrolyte, as shown in Figure S2. The difference should be attributed to the structural stability of a surface film on the electrode as mentioned above.

In the conventional evaluation method of rate capability, it is difficult to discriminate the reason for capacity decay under high current density. To exclude the capacity decay caused by electrode degradation, we investigated the rate capability of the annealed Ni–P/(etched Si) electrode with charge capacity limit in the FSA-based electrolyte (Figure S3). A discharge capacity of 1000 mA h g^{-1} was maintained until a current rate of 2.0 *C*. Although capacity decay was observed at 5.0 *C*, the capacity was recovered when the current rate was back to 0.1 *C*. This result suggests that the capacity decay is caused by limitation of mass transfer. The capacity of 1000 mA h g^{-1} was retained while hardly effecting mass transfer until 2.0 *C*. Therefore, the electrode in the FSA-based electrolyte would stably cycle until a relatively high rate of 2.0 *C*.

To reveal the reason for the difference in the cycle stability of the annealed Ni–P/(etched Si) electrode (Figures 1b), we observed the surface morphology by FE-SEM. Figures 2a–2d show FE-SEM image of the electrode surface after 1 and 50 cycles. No cracks were observed on the electrode surface after the 1st cycle regardless of electrolyte (Figures 2a and 2c), which suggests that the Ni–P coating layer alleviates the stresses arising from the change in the volume of Si layer during the charge–discharge reaction.[24] On the other hand, the crack generated on the electrode surface after the 50th cycle, as shown in Figures 2b and 2d. Since there is no great distinction between the TFSA- and FSA-based electrolytes, the reason for capacity decay in the TFSA-based electrolyte in Figure 1b cannot be explained by only surface morphology. Thus, EIS measurement was conducted to investigate electrochemical behavior of Li^+ at the interface between the electrode and the electrolyte.

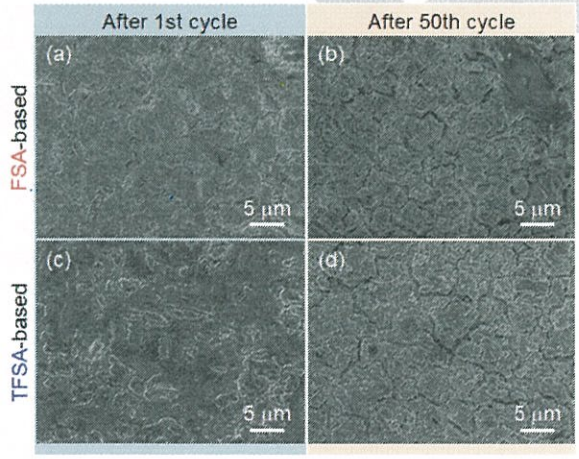

Figure 2. (a) FE-SEM images of annealed Ni–P/(etched Si) electrodes after (a, c) 1 or (b, d) 50 cycles. The electrodes were cycled in (a, b) 1 M LiFSA/PP1MEM-FSA or (c, d) 1 M LiTFSA/PP1MEM-TFSA.

Figures 3a and 3b display Nyquist plots of the annealed Ni–P/(etched Si) electrodes charged at 0.005 V vs. Li^+/Li after 10 cycles in each electrolyte. Solution resistance (R_{sol}) corresponds to ionic conductivity of the electrolyte, which reflects Li^+ transport in the bulk of electrolyte. The first semicircle in the high frequency region denotes interfacial resistance (R_{if}) which is associated with interfacial Li^+ transfer processes. They include desolvation of anions from Li^+ as well as Li^+ transport in an electrical double layer and/or surface layer induced by the decomposition of electrolyte.[25] The second semicircle corresponds to charge transfer resistance (R_{ct}), and is related to a Li–Si alloying reaction.[26] The straight line with a slope of approximately 45° at low frequency called Warburg impedance (Z_w) is derived from solid state diffusion of Li in a Si layer.[26] Resistances of these components were analyzed by using an equivalent circuit as shown in Figure 3c, and calculated resistances are summarized in Table 1. R_{sol} in the FSA-based electrolyte was nearly one third of that in the TFSA-based electrolyte, which is attributed to difference in conductivity of each electrolyte.[23] R_{if} in the FSA-based electrolyte was much less than that in the TFSA-based electrolyte, which indicates that Li^+ transferred smoothly at the electrode–electrolyte interface. In addition, R_{ct} was lower in the FSA-based electrolyte. This suggests that Li–Si alloying reaction easily occurs due to smooth

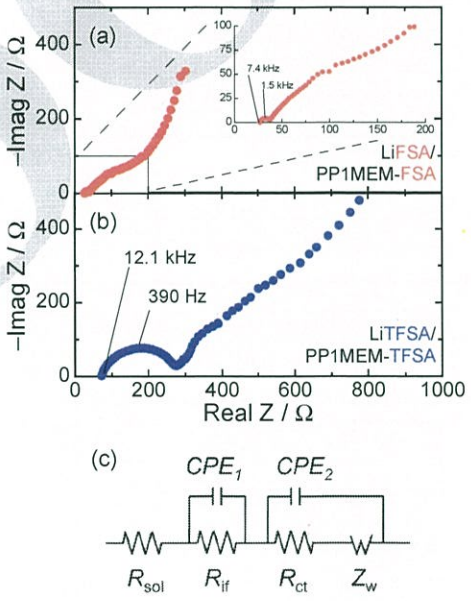

Figure 3. Nyquist plots of the annealed Ni–P/(etched Si) electrode at the 10th charged state (0.005 V vs. Li^+/Li) in 1 M (a) LiFSA/PP1MEM-FSA and (b) LiTFSA/PP1MEM-TFSA. (c) Equivalent circuit for impedance analysis in this study.

Table 1. Summary of impedance of annealed Ni–P/(etched Si) electrodes after 10 cycles estimated in Figure 3 and conductivity of ionic liquid electrolytes.[23]

Electrolyte	R_{sol}/Ω	R_{if}/Ω	R_{ct}/Ω	Conductivity[23] /mS cm^{-1}
FSA-based	26.1	8.8	78.5	2.06
TFSA-based	72.0	210	260	0.66

Li^+ supply to the interface. However, care must be taken that an EIS spectrum for a two-electrode cell includes information from both electrode/electrolyte interfaces. To discuss more correctly, we performed EIS measurement for a Li/Li symmetric cell in each electrolyte and Figure S4 shows the results. Although all resistances in the FSA-based electrolyte was lower than those in the TFSA-based electrolyte, the difference was smaller than the results of annealed Ni–P/(etched Si) three-electrode cells. Therefore, we concluded that the resistances of annealed Ni–P/(etched Si) certainly were reduced in the FSA-based electrolyte. These lower R_{sol}, R_{if} and R_{ct} should lead to high cycle performance and good rate capability. We considered that this difference in resistance is attributed to the coordination environment around Li^+ and the properties of the surface film formed on the annealed Ni–P/(etched Si) electrode. We have demonstrated that the ionic association tendency of the Li salt corresponds to the desolvation of the anion from Li^+ more easily occurs in the FSA-based electrolyte.[23] This should be the reason why R_{if} and R_{ct} in the FSA-based electrolyte is lower.

In summary, we investigated the effect of the anion structure in an ionic liquid electrolyte on the electrochemical performance of an annealed Ni–P/(etched Si) negative electrode for LIBs. The electrode showed better cycle performance and rate capability in the FSA-based electrolyte than those in the TFSA-based electrolyte. The surface morphology of the electrode after the cycles was almost the same regardless of electrolyte. On the other hand, R_{sol} of the FSA-based electrolyte was lower, contributing to high rate performance. In addition, lower R_{if} and R_{ct} enhances cycle performance, which is attributed to relatively facile desolvation of FSA^- from Li^+. As a consequence, the FSA-based ionic liquid electrolyte is able to improve the electrochemical performance of the annealed Ni–P/(etched Si) electrode, and contributes to realization of next-generation LIBs with a Si-based negative electrode.

This work was partially supported by the Japan Society for the Promotion of Science (JSPS) KAKENHI, grant Numbers JP17H03128, JP17K17888, JP16K05954. The authors thank Ryoji Inoue and Ken Asada (Hitachi Metals Neomaterial Ltd.) for their assistance with the synthesis of Ni–P/Si powders.

Supporting Information is available on http://dx.doi.org/10.1246/cl.180649.

References

1 C. J. Wen, R. A. Huggins, *J. Solid State Chem.* **1981**, *37*, 271.
2 B. Key, R. Bhattacharyya, M. Morcrette, V. Seznéc, J.-M. Tarascon, C. P. Grey, *J. Am. Chem. Soc.* **2009**, *131*, 9239.
3 W. Wang, P. N. Kumta, *ACS Nano* **2010**, *4*, 2233.
4 X. H. Liu, L. Zhong, S. Huang, S. X. Mao, T. Zhu, J. Y. Huang, *ACS Nano* **2012**, *6*, 1522.
5 H. Usui, K. Meabara, K. Nakai, H. Sakaguchi, *Int. J. Electrochem. Sci.* **2011**, *6*, 2246.
6 H. Usui, N. Uchida, H. Sakaguchi, *Electrochemistry* **2012**, *80*, 737.
7 Y. Domi, H. Usui, M. Narita, Y. Fujita, K. Yamaguchi, H. Sakaguchi, *J. Electrochem. Soc.* **2017**, *164*, A3208.
8 H. Usui, K. Wasada, M. Shimizu, H. Sakaguchi, *Electrochim. Acta* **2013**, *111*, 575.
9 K. Hayamizu, S. Tsuzuki, S. Seki, *J. Chem. Eng. Data* **2014**, *59*, 1944.
10 H. Matsumoto, H. Sakaebe, K. Tatsumi, *ECS Trans.* **2009**, *16*, 59.
11 S. Tsuzuki, K. Hayamizu, S. Seki, *J. Phys. Chem. B* **2010**, *114*, 16329.
12 N. Dupré, P. Moreau, E. D. Vito, L. Quazuguel, M. Boniface, H. Kren, P. Bayle-Guillemaud, D. Guyomard, *Chem. Mater.* **2017**, *29*, 8132.
13 M. Shimizu, H. Usui, K. Matsumoto, T. Nokami, T. Itoh, H. Sakaguchi, *J. Electrochem. Soc.* **2014**, *161*, A1765.
14 K. Yamaguchi, Y. Domi, H. Usui, H. Sakaguchi, *ChemElectroChem* **2017**, *4*, 3257.
15 K. Ababtain, G. Babu, X. Lin, M.-T. F. Rodrigues, H. Gullapalli, P. M. Ajayan, M. W. Grinstaff, L. M. R. Arava, *ACS Appl. Mater. Interfaces* **2016**, *8*, 15242.
16 S.-H. Baek, J.-S. Park, Y.-M. Jeong, J. H. Kim, *J. Alloys Compd.* **2016**, *660*, 387.
17 D. M. Piper, T. Evans, K. Leung, T. Watkins, J. Olson, S. C. Kim, S. S. Han, V. Bhat, K. H. Oh, D. A. Buttry, S.-H. Lee, *Nat. Commun.* **2015**, *6*, 6230.
18 V. Chakrapani, F. Rusli, M. A. Filler, P. A. Kohl, *J. Phys. Chem. C* **2011**, *115*, 22048.
19 P. C. Howlett, E. I. Izgorodina, M. Forsyth, D. R. MacFarlane, *Z. Phys. Chem.* **2006**, *220*, 1483.
20 B. Philippe, R. Dedryvère, M. Gorgoi, H. Rensmo, D. Gonbeau, K. Edström, *J. Am. Chem. Soc.* **2013**, *135*, 9829.
21 I. A. Shkrob, Y. Zhu, T. W. Marin, D. Abraham, *J. Phys. Chem. C* **2013**, *117*, 19255.
22 V. Etacheri, O. Haik, Y. Goffer, G. A. Roberts, I. C. Stefan, R. Fasching, D. Aurbach, *Langmuir* **2012**, *28*, 965.
23 K. Yamaguchi, Y. Domi, H. Usui, M. Shimizu, K. Matsumoto, T. Nokami, T. Itoh, H. Sakaguchi, *J. Power Sources* **2017**, *338*, 103.
24 C.-Y. Chen, T. Sano, T. Tsuda, K. Ui, Y. Oshima, M. Yamagata, M. Ishikawa, M. Haruta, T. Doi, M. Inaba, S. Kuwabata, *Sci. Rep.* **2016**, *6*, 36153.
25 C. C. Nguyen, S.-W. Woo, S.-W. Song, *J. Phys. Chem. C* **2012**, *116*, 14764.
26 Y. Yamada, Y. Iriyama, T. Abe, Z. Ogumi, *J. Electrochem. Soc.* **2010**, *157*, A26.